JOURNAL OF THEORETICAL
AND APPLIED MECHANICS
51, 4, pp. 903-913, Warsaw 2013

EFFECT OF CIRCUMFERENTIAL GROOVES CASING TREATMENT ON TIP LEAKAGE FLOW AND LOSS IN A TRANSONIC MIXED-FLOW COMPRESSOR

Xiao-Qing Qiang, Ming-Min Zhu, Jin-Fang Teng
School of Aeronautics and Astronautics, Shanghai Jiao Tong University, Shanghai, China
e-mail: jackzhushen@sjtu.edu.cn

A numerical simulation of a single stage transonic mixed-flow compressor is presented. The simulation is run with a multi-passage grid that models the 3D, viscous, steady and unsteady flow field. The effect of circumferential grooves casing treatment on the compressor overall performance, tip leakage flow and loss has been studied. The results show that the narrow operating range has been significantly broaden by the casing treatment grooves, while the mismatching between the rotor and stator still exists and becomes even worse. Detailed analysis indicates that the fluid from circumferential grooves is injected into the blade passage near the suction surface and re-energizes the leakage flow, which makes mainly contribution to manipulation of the tip leakage flow and stall margin improvement. Since the pressure difference across the blade tip section has a great impact on the effectiveness of circumferential grooves, the positions of shock wave and tip leakage flow as well as where the interaction takes place ought to be taken into account through the casing treatment design procedure.

Key words: compressor, casing treatment, tip leakage, flow loss, numerical simulation

Nomenclature

SC	–	smooth casing [–]
CT	–	casing treatment [–]
PE	–	peak efficiency [–]
NS	–	near stall [–]
SM	–	stall margin [–]
π	–	pressure ratio [–]
$\dot{m}$	–	mass flow rate [kg/s]
Zone 1, 2	–	low momentum region near leading and trailing edge, respectively [–]
TLF 1, 2	–	tip leakage flow from fore and rear chord, respectively [–]

1. Introduction

Mixed-flow or diagonal-flow compressor stages have been regarded as providing advantages over both axial and centrifugal compressors. Combining these merits of high pressure ratio, a wide operating range and small frontal area, mixed-flow compressors have a bright prospect of application of small-sized military/civil turbofan or turbo-shaft engines.

In the late 1950s, several research works about the design and performance test of mixed-flow compressor stages were conducted (Goldstein, 1948; Osborn and Hamrick, 1952). Along with the rapid development of axial and centrifugal compressor design techniques, transonic mixed-flow compressors with high rotating speeds and pressure ratios were designed and studied since the 1980s (Musgrave and Plehn, 1987; Mönig *et al.*, 1993). The increasing rotor blade loading and tip tangential velocity, Mach number at the inlet blade tip resultes, in consequence, a higher loss

and intensive interaction between the shock wave and tip leakage flow as well as boundary layer, which made a great impact on the endwall flow stability in modern transonic compressors.

Dominant features of the compressor endwall flow include the tip leakage flow; interactions among the tip leakage flow, the passage shock and the endwall boundary layers; and accumulation of the low momentum fluid due to radial migration (Hah *et al.*, 2010). Particularly, flow characteristics of the tip leakage flow keep attracting considerable attention from researchers. A great number of experimental and computation studies on the tip leakage flow in transonic compressors were reported (Hah *et al.*, 2010; Suder and Celestina, 1994; Hah and Rabe, 2001). The tip leakage flow as well as its interaction with the shock wave manifests intensive unsteady characteristics and are considered as a key role in compressor stall inception. Additionally, some studies have proposed tip leakage vortex breakdown as a possible cause of stall inception in transonic compressors (Schlechtriem and Loetzerich, 1997; Hoffman and Ballman, 2003). Breakdown of the tip leakage vortex occurs downstream the shock wave at the near stall condition, leading to large blockage effect near the tip and also the unsteady flow phenomena in the rotor passage, which may be related to the spillage of the tip leakage flow at the stall inception (Yamada *et al.*, 2007).

Casing treatments have proved adequate to manipulate the specific flow mechanisms which are responsible for compressor stall and, thereby, enhance the stall margin. Numerous studies of casing treatment applied to transonic compressors have been carried out to identify the fundamental flow mechanisms and their influence on the operating range enhancement as well as flow stabilization (Hembera *et al.*, 2008; Beheshti *et al.*, 2004; Wilke *et al.*, 2005). A better understanding of the complex flow characteristics has been achieved through time-resolved simulations and accurate measurements such as fast response pressure transducer and PIV technique (Voges *et al.*, 2011). Circumferential-groove casing treatments have been applied very successfully to certain transonic compressors with a moderate stall margin enhancement and acceptable efficiency penalty. Particularly, recent researches reported that grooves with a much smaller depth than conventional designs are shown to be similarly effective in increasing the stall margin, and the stage efficiency at design speed is shifted to slightly higher values (Müller *et al.*, 2007).

This paper documents a numerical study of a single stage transonic mixed-flow compressor aimed at addressing these issues. By both steady and unsteady simulation, the behavior of tip leakage flow and its influence on the stall process are specifically discussed. The flow phenomena changes caused by the circumferential grooves casing treatment are emphasized in detail.

2. Descriptions of investigated model and numerical method

The present study is based mainly on numerical simulation carried out by Numeca/FINE. The investigated mixed-flow compressor stage is a transonic front stage of a four-stage high-pressure compressor. It consists of a low-aspect-ratio blisk rotor equipped with 21 blades (with 1% blade height tip clearance, 3mm hub fillet) and a stator with 49 typical straight blades. The inlet relative Mach number at the rotor tip reaches 1.4 at the design condition, whereas the hub runs at subsonic conditions. Figure 1 illustrates the cross section of this transonic mixed-flow compressor stage.

The casing treatment consisted of five grooves lies between 10% and 94% of the rotor axial chord. Since a deeper groove produces a higher efficiency loss, a moderate-depth (6 mm) groove configuration is chosen. All of the grooves in a given configuration have the same shape. According to the previous study, the ratio of the groove width to gap between each groove has to be larger than 2 (Prince *et al.*, 1974). To fulfill the requirement, the axial extent of the groove is chosen to be 12% of the rotor axial chord, while the gap length to be 6%. A schematic of the casing treatment grooves is presented in Fig. 2.

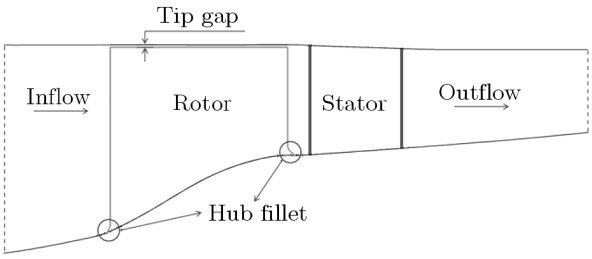

Fig. 1. Cross section of the mixed-flow compressor stage

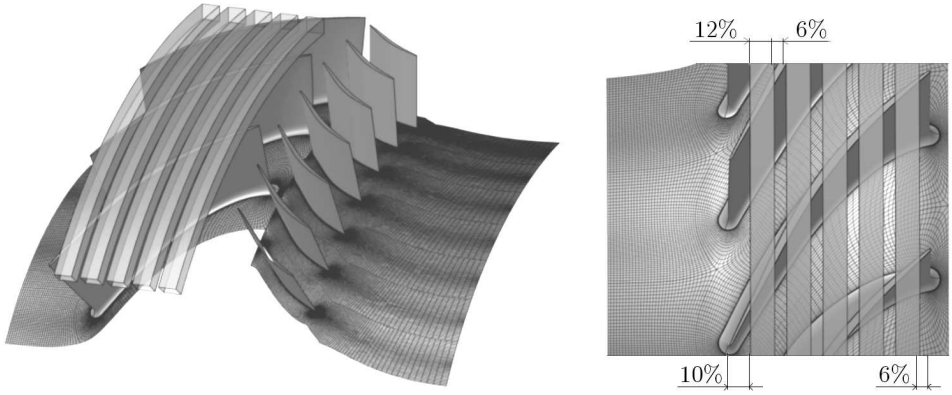

Fig. 2. Schematic of the casing treatment grooves

Both steady and unsteady numerical simulations were performed. In particular, the domain scaling approach was applied in the unsteady simulation. Considering the constraints of this approach (rotor/stator periodicities must be equal), 3 rotor passages and 7 stator passages (shown in Fig. 2) were simulated in total so as to identify the behavior of the tip leakage flow and to capture instantaneous flow structures near stall more accurately. A number of 4.73 million grid points was used, including 1.33 million grid points in the rotor blade passage, 2.89 million in the stator passage, 0.16 million in the tip clearance, and additional 0.35 million in the casing treatment grooves. The rotor and stator blades were meshed in H-O-H topology, while the rotor tip clearance geometry was meshed with a butterfly topology. The circumferential grooves were modeled in a separated block with straight H-block. For each groove, 65 nodes in the tangential direction, 33 nodes in radial and 33 nodes in axial were used to represent the groove geometry.

The RANS equations were discretized in space using a cell-centered explicit finite volume scheme. Spalart-Allmaras model was applied to introduce turbulence. The steady-state flow solution was achieved at the convergence of a fourth-order explicit Runge-Kutta integration scheme. The time-marching algorithm was stabilized using scalar eigenvalue-based second-order and fourth-order difference smoothing operators. Unsteady simulations were implemented in the Jameson implicit dual time-stepping scheme, which allowed for the solution of a steady state problem at each physical time step. This methodology enables keeping the main advantages of the explicit time integration scheme already implemented for resolving steady-state problems as well as retaining the local time stepping and implicit residual smoothing. For the time dependent simulation, 30 physical time steps per stator passage and 50 pseudo-time iterations with a CFL number of 3 within each physical time step were performed. The local time stepping, implicit residual smoothing and multigrid techniques were applied to reduce the computation cost.

At the inlet, the flow direction was assumed to be axial. A constant total pressure of 101 325 Pa and a constant total temperature of 288.15 K were applied. At the outlet, the average static pressure was given at a channel extension downstream the stator row to avoid numerical reflections. The side boundaries of the passage were modeled with matching periodicity. Solid boundaries were applied at the hub, casing and blade surfaces with no slip and impermeability conditions.

3. Results and discussions

3.1. Effect of the casing treatment on compressor performance

The compressor speed line was obtained by raising the exit back pressure incrementally. When closing to the stall point, the converged solution of the last point was used as the initial solution. The mass flow rate continued to decrease with rising the exit back pressure until the convergent solution no longer existed. The last steady and converged solution point would be considered as the near stall (NS) point.

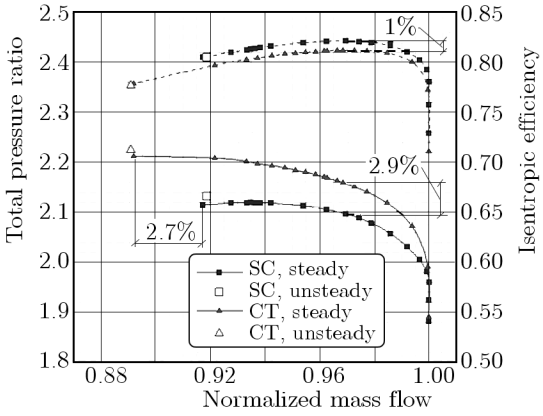

Fig. 3. Overall performance for the compressor stage at 100% design speed

Figure 3 presents the overall performance for the mixed-flow compressor stage at 100% design speed both with the smooth casing (SC) and casing treatment (CT). As a comparison, the unsteady solutions at NS condition are also marked in the figure. The total pressure ratio and isentropic efficiency are plotted as a function of the mass flow. The figure shows a peak efficiency (PE) of 0.8215 and maximum total pressure ratio of 2.119 with SC. At PE mass flow, the total pressure ratio reaches 2.097. At a normalized mass flow of 91.7%, the last steady converged solutions are gained with a pressure ratio of 2.114. As shown in Fig. 3, values of unsteady solution are almost equal to the steady solution at NS condition. Thus, in consideration of computation economy, the compressor speed line is attained by steady solutions. The stall margin is calculated by

$$\mathrm{SM} = \left(\frac{\pi_{\mathrm{NS}}/\dot{m}_{\mathrm{NS}}}{\pi_{\mathrm{PE}}/\dot{m}_{\mathrm{PE}}} - 1\right) \cdot 100\% \tag{3.1}$$

where π and $\dot{m}$ are the value of total pressure ratio and mass flow rate at NS or PE conditions. Hence, this mixed-flow compressor with SC gains a stall margin of 6.57%, which is badly in need of improving.

Seen from the figure, the impact of casing treatment on the mixed-flow compressor stage performance is just obvious. The casing treatment consisting of 5 moderate-depth grooves is able to enhance the compressor flow stability effectively with a slight drop of 1% in the isentropic efficiency at PE mass flow. Furthermore, the casing treatment raises the stage total pressure ratio significantly. The normalized stall mass flow reduces by 2.7% and total pressure ratio increases by 2.9% at PE mass flow. Thus, the SM with CT rises to 11.25%, 1.7 times from the stall margin with SC, according to Eq. (3.1). As the mass flow decreases from PE to NS condition, the growth of total pressure ratio keeps increasing.

In order to evaluate the influence of the casing treatment on the main passage flow, pitch averaged radial profiles of several flow parameters are discussed at PE and NS conditions. Figure 4 presents the spanwise distributions of total pressure ratio as well as isentropic efficiency

at the rotor outlet and incidence angle at the stator inlet. Apparently, the installation of this circumferential casing treatment has a noticeable impact on these flow parameters. Figure 4a shows a pretty high aerodynamic loading near the tip region both at PE and NS conditions with SC. Dramatic growth of the total pressure ratio is observed above 70% span. At NS condition, the maximum pressure ratio near the tip region is about 3% higher than that at PE condition at the same span. With CT, the maximum magnitude is achieved at 75% span, much lower than 95% span of SC case, which means the highly loaded region is shifted to a lower position by casing treatment. Furthermore, the pressure ratio below 85% span rises remarkably in comparison with SC case, especially at NS condition. The greatest growth in the total pressure ratio at NS condition comes up to about 9.5% at 73% span. In Fig. 4b, efficiency drop owing to casing treatment is noticed above 70% and 60% span at PE and NS conditions respectively, and the difference resulted from CT at NS condition is larger than that at PE condition. These changes along the spanwise indicate that the region influenced by CT on the efficiency distribution lies above higher span near the tip region, contributing to the efficiency drop shown in the compressor performance map. Figure 4c shows the impact of casing treatment on the incidence at the stator inlet. At PE condition, the incidence angle distribution does not change a lot with CT. However, it increases by 2° to 6° in a wide range of span at NS condition. Although this casing treatment configuration is capable of enhancing the flow stability and rising pressure ratio for the investigated mixed-flow compressor effectively, it aggravates the incidence distribution at NS condition rather than improving the matching status between the rotor and stator.

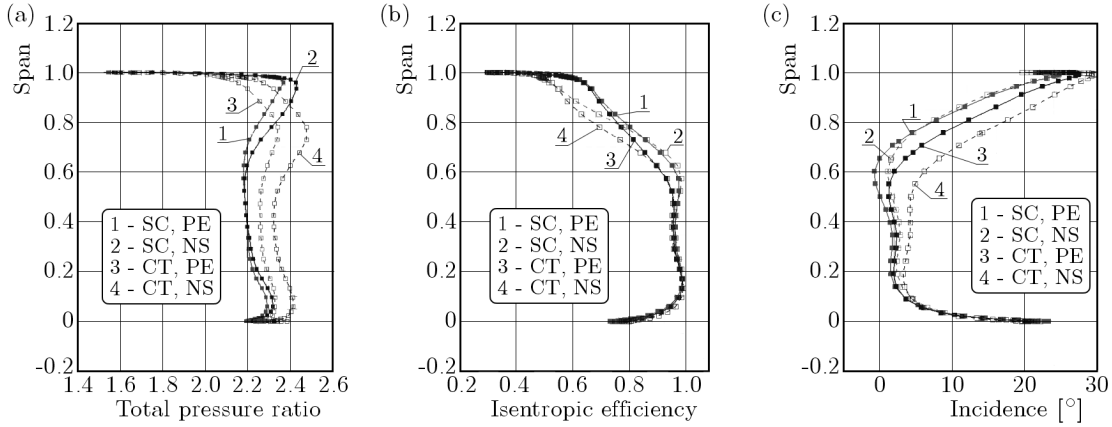

Fig. 4. Spanwise distributions of performance at PE and NS conditions; (a) total pressure ratio at the rotor outlet, (b) isentropic efficiency at the rotor outlet, (c) incidence angle at the stator inlet

3.2. Tip blockage and tip leakage flow with SC

Figure 5 shows the comparison of the relative Mach number distribution between PE and NS conditions at 98% span. At PE condition, a small area of low momentum (Zone 1) has already formed behind the detached shock wave, nearly in the middle of tip passage, followed by a much larger one (Zone 2) closed to the pressure surface. The shock-boundary layer interaction can also be observed near the blade suction side. As the mass flow decreases to NS condition, Zone 1 as well as Zone 2 grows larger, and Zone 1 in the middle of the tip passage moves further upstream and towards the pressure surface, almost reaching the leading edge. The detached shock wave is pushed away from the leading edge by the increased back pressure, thereby the position where the shock wave interacts with the boundary layer moves forward from 33% to 29% of the rotor axial chord.

Figure 6 presents the tip leakage vortex and leakage flow inside the blade passage at two conditions with particle traces released from the region 0.6% axial chord downstream the leading edge. The color of particle traces describes its velocity. The isolines of the relative Mach number

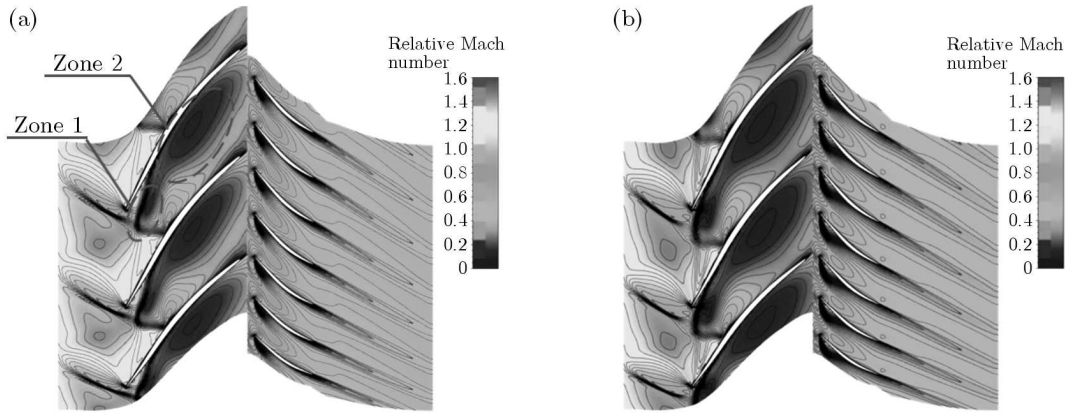

Fig. 5. Relative Mach number at 98% span; (a) PE condition, (b) NS condition

ranging from 0.99 to 1.01 at 98% span are also plotted in black lines to represent the shock wave.

At PE condition, as described in Fig. 6a, the tip leakage vortex core is formed by the fluid originating near the blade tip section, as the consequence of the pressure difference between the pressure and suction side at the blade tip. Once the trajectory of vortex core encounters the shock wave, the velocity of particle traces drops dramatically with a remarkable enlargement of vortex diameter. This phenomenon is supposed to be the onset of so-called vortex breakdown, which could be a triggering of stall inception (Hoffman and Ballman, 2003). Right behind the shock wave, the tip leakage flow originating from the leading edge (TLF 1) strides over the blade tip perpendicularly to the main flow direction at the position between about 30% to 40% axial chord and travels above the core vortex. This leakage flow rolls up around the vortex core and forms the induced tip leakage vortex. After passing through the middle of the blade tip passage, TLF 1 turns direction sharply into main flow and moves towards the pressure surface of the adjacent blade passage near the tailing edge. The direction-changing area forms the small-sized low momentum zone (Zone 1) shown in Fig. 5a. Both vortex core and leakage flow move radially inward as they move downstream. Another part of the tip leakage flow (TLF 2) strides over the blade tip between 40% to 84% axial chord and moves towards the pressure surface, above the vortex core and TLF 1. The vortex core and two parts of the leakage flow accumulate at the middle and the rear portion of the blade passage near the pressure surface and concur to bring about the formation of the large-sized low momentum region (Zone 2).

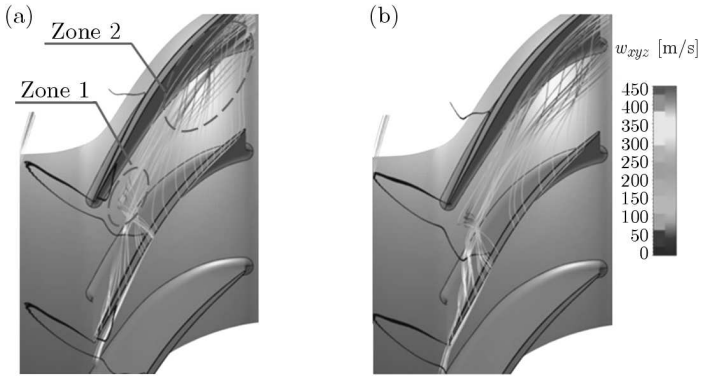

Fig. 6. Particle traces near rotor tip; (a) PE condition, (b) NS condition

As the mass flow reduces to NS condition, since the tip leakage vortex core strengthens and becomes more parallel to the leading edge plane, the shock wave has been pushed upstream (seen Fig. 6b). The vortex core encounters the shock frontier at 13% of the axial chord downstream the

leading edge, earlier than 19% at PE condition. Besides, TLF 1 travels further across the blade passage than at PE condition, turning its direction into the main flow closer to the pressure surface. This tip leakage flow always rolls up around the vortex core right behind the shock wave, where the so-called vortex breakdown might occur. It implies that the vortex breakdown might make an effort to drive the tip leakage flow to stride over the tip clearance in the direction perpendicular to the main flow besides the pressure difference across the tip clearance.

The phenomena of "blade tip stall" and "tip blockage stall" have been identified as the two basic classes of tip stall mechanisms in transonic compressors (Brignole *et al.*, 2005). Based on the previous description of these two phenomena, the tip stall mechanism in this compressor stage is supposed to be the "tip blockage stall" one. The present paper is focused on this aspect. The effect of tip leakage flow is taken into account to improve the understanding of the "tip blockage stall" (as Fig. 7 shows). The tip leakage flows can be divided into two types according to the leaking position and flow behavior inside the blade passage. Both two types play an indispensable role in formation of the low momentum area (Zone 1 and 2). The radial inward moving and direction-changing of TLF 1, which might be induced by vortex core breakdown, results in low momentum area Zone 1, as the "blockage of inflow" mentioned by Brignole *et al.* (2005). The vortex core as well as TLF 1 and 2 arrives at the middle and rear part of the blade passage near the pressure surface at a low velocity, jointly leading to the formation of Zone 2, as the "vortex stagnation zone" in the previous research. Since the vortex core breakdown and tip leakage flow are relevant to the "tip blockage stall", the application of casing treatment should be able to manipulate such flow behavior.

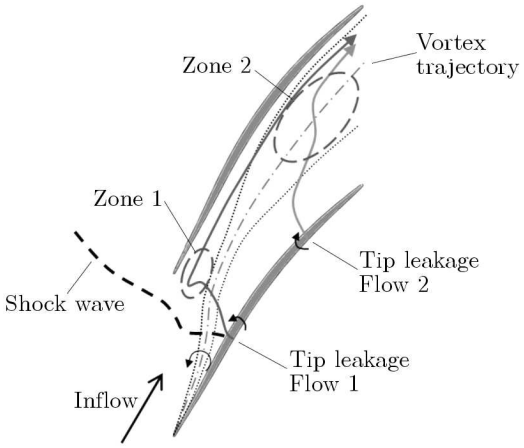

Fig. 7. The effect of tip leakage flow on the tip blockage stall mechanism at NS condition

3.3. Effect of the casing treatment on tip leakage flow

The flow field details of casing treatment case at smooth casing PE mass flow rate (91.7% of choked mass flow) calculated by steady simulation are discussed here. The relative Mach number contour at 98% span and particle traces near rotor tip are presented in Fig. 8. Compared with Fig. 5a, which is at the same mass flow level, it is observed that the low momentum area Zone 1 and 2 no longer exists at 98% span. The blockage inside the blade passage has been dampened or vanished dramatically after the installation of casing treatment. Particle traces in Fig. 8b, also originating from the region of 0.6% of the axial chord downstream the leading edge, shows that the position where the shock wave interacts with the tip leakage vortex moves further downstream compared with Fig. 6a. Besides, the trajectory of the tip leakage vortex core moves more towards the suction surface. No more leakage flow behaving in the same way as TLF 1 is found in SC case, providing an explanation to the repression of blockage Zone 1. The vortex core and tip leakage flow exit the blade passage in a higher velocity than in SC case at 98%

span, which weakens the low momentum area Zone 2. Hence, it can be concluded that this configuration consisting of 5 grooves can effectively manipulate the flow behavior of the tip leakage vortex and leakage flow, depress the tip blockage and, therefore, delay the occurrence of stall inception.

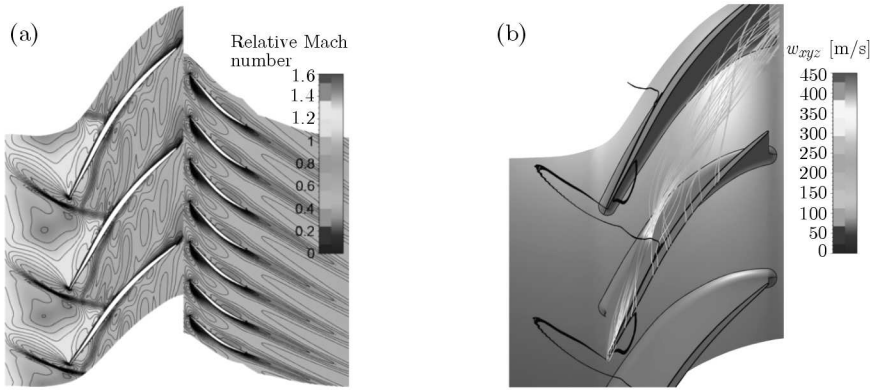

Fig. 8. Relative Mach number at 98% span and particle traces near the rotor tip at smooth casing PE condition; (a) relative Mach number at 98% span, (b) particle traces near rotor tip

Entropy distributions on a series of cross-flow planes with particle traces near the rotor tip with SC and CT are compared at smooth casing PE condition in Fig. 9. Particle traces presenting the tip leakage vortex originating from the leading edge are painted in light color, while the tip leakage flow is painted in deep color, originating from the region very close to the pressure surface at 98% span, from approximately 30% to 40% of the axial chord. As previously mentioned, particle traces in deep color, regarded as the TLF 1, enters the blade passage from the pressure surface and moves upstream and radially inward. Then TLF 1 arrives in the middle of the tip passage at a low speed (seen in Fig. 6a) and turns its direction into main flow. Figure 9b shows changes in the flow field with 5 CT grooves. Particle traces, starting from the same position as in Fig. 9a, turn into main flow right after striding over the blade tip and roll up around the leakage vortex core (in light color). Consequently, the leakage flow in CT case passes through the blade passage closer to the suction surface than that in SC case.

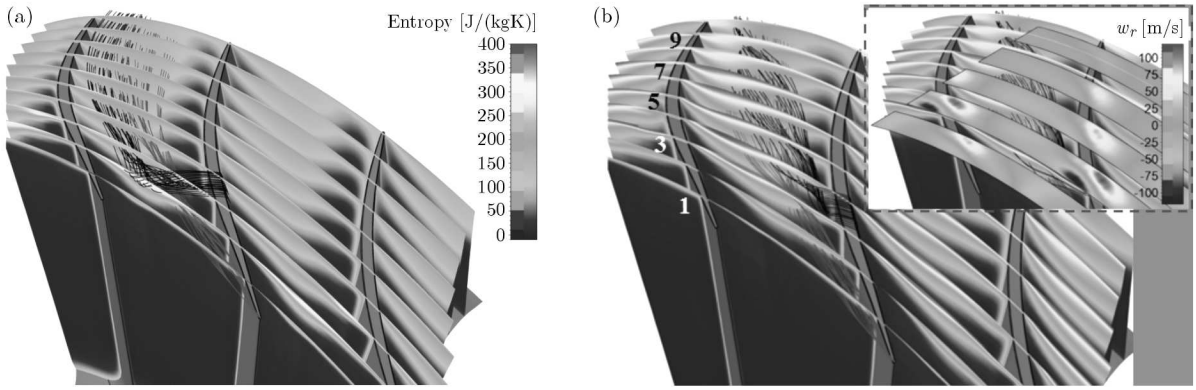

Fig. 9. Entropy distributions on cross-flow planes and particle traces near the rotor tip at smooth casing PE condition; (a) with SC, (b) with CT

3.4. Effect of casing treatment on loss at the rotor tip

Figure 9a shows a high loss region at the 2nd cross-flow plane downstream the leading edge, near the position where TLF 1 changes its direction, as a consequence of a low speed flow and the resulting blockage here. Owing to manipulation of the tip leakage flow by casing treatment,

Zone 1 resulted from TLF 1 is remarkably damped as well as Zone 2, as depicted in Fig. 8a. However, much higher loss regions are observed at the top of 3rd to 7th planes downstream the leading edge, very close to the endwall. 8th to 10th planes also show higher and wider loss regions than that in SC case. Since the leakage flow does not pass through these high loss regions, the applied casing treatment is supposed to be the dominant because of high loss near the endwall. The radial velocity distribution at the interface between the rotor casing and circumferential grooves is also shown in Fig. 9b. The positive radial velocity zone in each groove is located very close to the pressure surface of the tip passage, while negative zones near the suction surface. Circumferential grooves draw the fluid near the pressure surface out of the blade passage and feed it back near the suction surface, bringing about complex interactions between the main flows and casing treatment, which certainly have a great impact on endwall flow and causes high loss regions.

On the one hand, the introduction of circumferential casing treatment manipulates the tip leakage flow behavior and, consequently, removes the tip blockage Zone 1 and 2, reducing the tip blockage loss. On the other hand, interactions between the blade passage flow and casing treatment result in a high loss region near the endwall. Whether the circumferential casing treatment can increase or decrease the overall efficiency depends on the combined effect of all these factors. In addition, the influence of casing treatment on the efficiency ranges from the casing to the middle-upper span according to Fig. 4b, not only limited to the tip region. More future work needs to be given to evaluate the loss variation caused by CT quantitatively, in order to optimize the design of circumferential casing treatment with less efficiency drop.

3.5. Re-energizing process and its role in casing treatment design

In Fig. 9b, zones with the maximum magnitude of positive and negative radial velocity are both located in Groove 2 from the leading edge as a result of the greatest change in pressure difference across the blade tip section. The negative radial velocity zone in Groove 2 just lies above the area of fairly low static pressure near the detached shock wave. The fluid migrating circumferentially inside the groove is re-injected into the main flow at the low pressure location, where TLF 1 passes through in SC case. The fluid from the groove re-energizes TLF 1 and enforces it into the main flow directly, interpreting the depression of the low momentum zone and flow blockage caused by TLF 1. Except Groove 5, the left three grooves show both obvious positive and negative radial velocity zones, making the removal/injection procedure possible. It implies that the pressure difference across the blade tip section near the trailing edge is not adequate to complete the fluid transport. Compared with the highly loss regions in the front part of the blade tip passage, lower losses at the top of 8th to 10th planes also provide an evidence of weak interaction between main the flow and Groove 5. Since Groove 5 lacks the capacity of re-energizing the leakage flow with only a highly loss at the tip region, the casing treatment of front 4 grooves is expected to be a better configuration on this mixed-flow compressor stage.

Unsteady simulation at NS condition with CT provides the time-averaged radial velocity distribution at the interface between the casing and grooves in Fig. 10. Particle traces near the rotor tip and isolines of the shock wave are also presented. Due to the increased back pressure at NS condition, the shock wave is pushed further upstream as well as the position where the interaction with the tip leakage vortex occurs. As a result, the maximum magnitude of negative radial velocity is achieved in Groove 1, above where the interaction between the shock wave and tip leakage vortex takes place. Owing to the upstream motion of the passage shock, a lower pressure difference is achieved across the blade tip section beneath Groove 2. In consequence, Groove 2 no longer provides enough energy to drive TLF 1 into the main flow directly. Backflow of TLF 1 is observed after entering the blade passage, and it turns back into the main flow direction pretty close to the adjacent pressure surface. It is not difficult to expect that as the

mass flow continues to decrease, the shock wave keeps moving upstream and provides a much less driving force to complete the injection procedure in Groove 2. Thus TLF 1 without enough re-energizing keeps moving upstream and brings about the low momentum region as Zone 1 again, making an effort to the onset of the stall process. The above discussion reveals that the pressure difference across the blade tip section determines the impact of circumferential grooves on the flow field and overall performance to some degree. Specifically, the positions of the shock wave and tip leakage flow as well as where the interaction takes place ought to be taken into account through the design procedure of circumferential grooves.

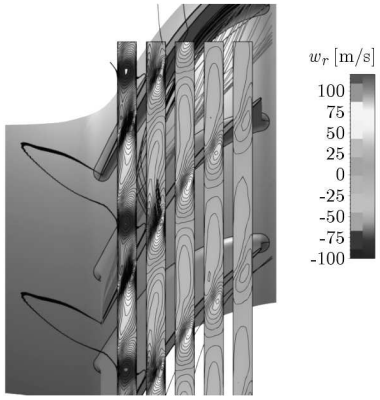

Fig. 10. Time-averaged radial velocity distribution at the interface between the casing and grooves and particle traces near the rotor tip at casing treatment NS condition

4. Conclusions

A mixed-flow compressor stage with and without casing treatment has been numerically simulated to study the effect of circumferential grooves casing treatment on the tip leakage flow and loss. By analyzing the detached shock wave, the tip leakage vortex and leakage flow as well as the interaction among them, the following conclusions have been drawn:

- The shock wave, tip leakage vortex and leakage flow concur to bring about the formation of two low momentum regions. Induced by pressure difference and shock-leakage vortex interaction, the tip leakage flow from the fore chord moves upstream and builds up a blockage zone at the pressure surface near leading edge;
- The circumferential grooves casing treatment is capable of enhancing flow stability and raising pressure ratio on the investigated mixed-flow compressor stage effectively. However, it aggravates the incidence distribution at NS condition rather than improving the matching status between the rotor and stator. It manipulates the endwall flow field via re-energizing the tip leakage flow from the fore chord and drives it into the main flow. The impact of grooves on the low momentum fluid is closely corresponding with the position where the shock wave interacts with tip leakage vortex.

Acknowledgements

This work was supported by the Initiative Projects of SJTU Young Teachers under Grant No. 12X100040080.

References

1. Beheshti B.H., Teixeira J.A., Ivey P.C., Ghorbanian K., Farhanieh B., 2004, Parametric study of tip clearance-casing treatment on performance and stability of a transonic axial compressor, *Proceedings of ASME*, GT2004-53390

2. Brignole G., Kau H.P., Wilke I., 2005, Numerical evaluation of important parameters ruling the effectiveness of casing treatments in transonic compressors, *Proceedings of ISABE*, ISABE-2005-1095

3. Goldstein A.W., 1948, Design and performance of experimental axial-discharge mixed-flow compressor: I – Impeller design theory, *NACA-RM-E8F04*

4. Hah C., Rabe D.C., 2001, Role of Tip Clearance flows on flow instability in axial flow compressors, *Proceedings of ISABE*, ISABE Paper 2001-1223

5. Hah C., Voges M., Mueller M., Schiffer H.P., 2010, Characteristics of tip clearance flow instability in a transonic compressor, *Proceedings of ASME*, GT2010-22101

6. Hembera M., Danner F.C.T., Brignoley G.A., Kau H.P., 2008, Numerical design and optimization of casing treatments for transonic axial compressors, *Proceedings of AIAA*, AIAA-2008-5063

7. Hoffman W.H., Ballman J., 2003, Some aspects of tip vortex behavior in a transonic turbocompressor, *Proceedings of ISABE*, ISABE Paper 2003-1223

8. Mönig R., Elmendorf W., Gallus H.E., 1993, Design and rotor performance of a 5:1 mixed-flow supersonic compressor, *ASME Journal of Turbomachinery*, **115**, 3, 565-572

9. Musgrave D.S., Plehn N.J., 1987, Mixed-Flow Compressor Stage Design and test results with a pressure ratio of 3:1, *ASME Journal of Turbomachinery*, **109**, 4, 513-519

10. Müller M.W., Schiffer H.P., Hah C., 2007, Effect of circumferential grooves on the aerodynamic performance of an axial single-stage transonic compressor, *Proceedings of ASME*, GT2007-27365

11. Osborn W.M., Hamrick J.T., 1952, Design and test of mixed-flow impellers: I – Aerodynamic design procedure, *NACA-RM-E52E05*

12. Prince D.C., Wisler D.C., Hilvers D.E., 1974, Study of casing treatment stall margin improvement, *NASA CR-134552*

13. Schlechtriem S., Loetzerich M,, 1997, Breakdown of tip leakage vortices in compressors at flow conditions close to stall, *Proceedings of ASME*, 97-GT-41

14. Suder K.L., Celestina M.L., 1994, Experimental and computational investigation of the tip clearance flow in a transonic axial compressor rotor, *NASA TM-106711*

15. Voges M., Schnell R., Willert C., MÖNig R., Müller M.W., Zscherp C., 2011, Investigation of blade tip interaction with casing treatment in a transonic compressor – Part I: Particle image velocimetry, *ASME Journal of Turbomachinery*, **133**, 1, 011007

16. Wilke I., Kau H.P., Brignole G., 2005, Numerically aided design of a high-efficient casing treatment for a transonic compressor, *Proceedings of ASME*, GT2005-68993

17. Yamada K., Funazaki K., Furukawa M., 2007, The behavior of tip clearance flow at near-stall condition in a transonic axial compressor rotor, *Proceedings of ASME*, GT2007-27725

Manuscript received November 21, 2012; accepted for print March 5, 2013